

FINAL STATES IN $\gamma\gamma$ AND γp INTERACTIONS *

STEFAN SÖLDNER-REMBOLD

Albert-Ludwigs-Universität Freiburg, Fakultät für Physik, D-79104 Freiburg, Germany
 E-mail: stefan.soldner-rembold@cern.ch

The total hadronic $\gamma\gamma$ cross-section measured by L3 and OPAL and the apparent discrepancy between the results are discussed. OPAL measurements of jet and charged hadron production in $\gamma\gamma$ scattering and preliminary H1 results on π^0 production in γp scattering are also presented. The mechanism of baryon number transfer in γp interactions at HERA has been studied for the first time by H1.

1 Total Hadronic $\gamma\gamma$ Cross-Section

At high $\gamma\gamma$ centre-of-mass energies $W = \sqrt{s_{\gamma\gamma}}$, the total hadronic cross-section $\sigma_{\gamma\gamma}$ for the production of hadrons in the interaction of two real photons is expected to be dominated by interactions where the photon has fluctuated into a hadronic state. Measuring the W dependence of $\sigma_{\gamma\gamma}$ should therefore improve our understanding of the hadronic nature of the photon and the universal high energy behaviour of total hadronic cross-sections.

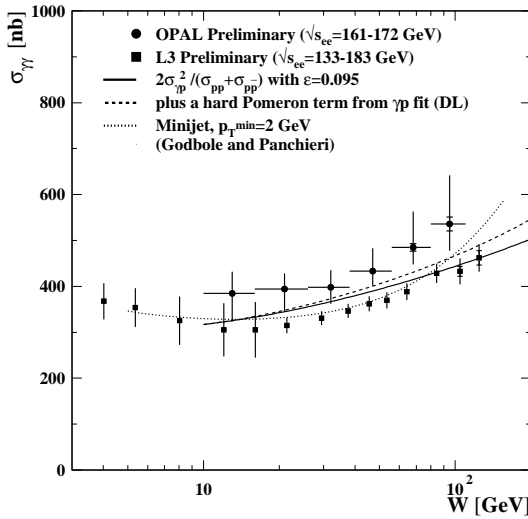


Figure 1: Total cross-section of the process $\gamma\gamma \rightarrow \text{hadrons}$ as a function of $W = \sqrt{s_{\gamma\gamma}}$. The inner error bars show the statistical errors and the outer error bars the quadratic sum of the statistical and systematic errors.

Before LEP2 the energy dependence of $\sigma_{\gamma\gamma}(W)$ had only been measured in the low energy region $W < 20$ GeV¹. These energies are too low to observe the high energy rise which is typical for hadronic cross-sections. Using the LEP2 data, L3² and OPAL³ have now measured $\sigma_{\gamma\gamma}(W)$ in the ranges $5 \leq W \leq 145$ GeV and $10 \leq W \leq 110$ GeV, respectively. The results are shown in Fig. 1.

*Talk given at ICHEP'98, Vancouver, Canada, July 22-30, 1998

Before interpreting these results, the apparent discrepancy between the OPAL and L3 measurements and the interpretation of the systematic errors require some discussion. OPAL shows the average of the results obtained by determining the detector corrections using either the Monte Carlo model PHOJET or PYTHIA and

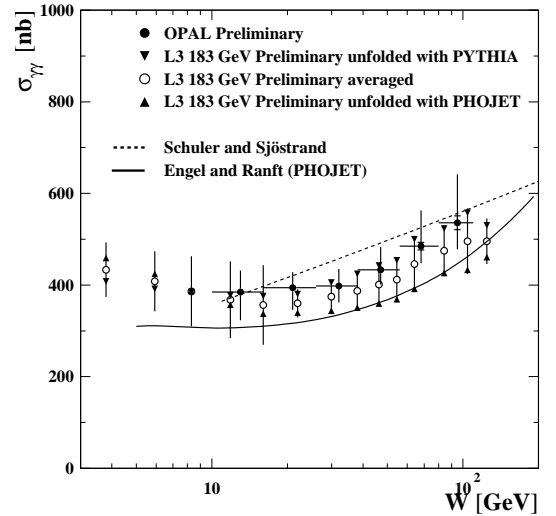


Figure 2: Comparison of the OPAL measurement with the average of the L3 results at $\sqrt{s_{ee}} = 183$ GeV obtained using PHOJET and PYTHIA (see text).

takes the difference between these results as part of the systematic error. L3 uses PHOJET to determine the central values and gives no model dependent systematic error. For $W < 20$ GeV the systematic errors become large in the case of L3 due to the finite trigger acceptance. OPAL avoids these regions by applying harder selection cuts. It should also be noted that the errors are highly correlated within one experiment. In order to make the two experiments more comparable, the L3 results for $\sqrt{s_{ee}} = 183$ GeV obtained with the PYTHIA and the PHOJET simulation of the detector, separately, are averaged in Fig. 2 and the full range is shown as vertical error bar. Comparing these results with the OPAL measurement shows that no significant discrepancy ex-

ists.

In Figs. 1 and 2, the results are compared to various theoretical predictions. The energy dependence of the total cross-sections for γp and hadron-hadron collisions is well described by a Regge parametrisation of the form

$$\begin{aligned}\sigma_{AB}(s) &= X_{AB}s^\epsilon + Y_{1AB}s^{-\eta_1} + Y_{2AB}s^{-\eta_2} \\ \sigma_{\bar{A}B}(s) &= X_{AB}s^\epsilon + Y_{1AB}s^{-\eta_1} - Y_{2AB}s^{-\eta_2}\end{aligned}\quad (1)$$

where \sqrt{s} is the centre-of-mass energy of the hadron-hadron or γp interaction and A, B denotes the interacting particles. The first term in the equation is due to Pomeron exchange and the other terms are due to C-even and C-odd Reggeon exchange⁴. The factors ϵ , η_1 and η_2 are assumed to be universal, whereas X_{AB} and Y_{iAB} are process dependent.

In a simple model, assuming factorisation of the Pomeron term X_{AB} , the total $\gamma\gamma$ cross-section can be related to the γp , pp and $\bar{p}p$ total cross-sections at high centre-of-mass energies $\sqrt{s}_{\gamma\gamma} = \sqrt{s}_{\gamma p} = \sqrt{s}_{pp} = \sqrt{s}_{\bar{p}p}$, where the Pomeron trajectory should dominate:

$$\sigma_{\gamma\gamma} = \frac{2(\sigma_{\gamma p})^2}{\sigma_{pp} + \sigma_{\bar{p}p}}. \quad (2)$$

The γp , pp and $\bar{p}p$ total cross-section are parametrised using Eq. 1. The universal factor $\epsilon = 0.095 \pm 0.002$ predicts a slow rise of the total cross-section with energy. Most models for the high energy behaviour of $\sigma_{\gamma\gamma}$ are based on similar factorisation assumptions for the soft part of the cross-section. This ansatz gives a reasonable description of the data (Fig. 1).

More sophisticated models predict a faster rise of $\sigma_{\gamma\gamma}(s)$ compared to the rise observed in hadron-hadron and γp interactions due to an additional ‘hard’ component in photon interactions. Donnachie and Landshoff (DL) propose an additional hard Pomeron term $\propto s^{0.4}$. In Fig. 1 the influence of this term is shown, if it had the same relative size as in γp scattering⁵. A mini-jet model, where the rise is driven by the increasing mini-jet cross-section⁶, is also shown. A faster rise is also predicted by the models of Schuler and Sjöstrand⁷ and the model of Engel and Ranft⁸ (Fig. 2). This faster rise is in qualitative agreement with the data. Fitting a Regge parametrisation to the data, L3 obtains $\epsilon = 0.158 \pm 0.006(\text{stat}) \pm 0.028(\text{sys})$ which is more than a factor 1.5 larger than the universal value².

Based on HERA measurements and assuming factorisation, quasi-elastic scattering ($\gamma\gamma \rightarrow \rho\rho$) and diffractive scattering (like $\gamma\gamma \rightarrow \rho X$) should contribute about 20–30% to the total hadronic $\gamma\gamma$ cross-section. Most of the final state hadrons in these processes are produced at very small polar angles. OPAL gives an acceptance between about 6% (using PYTHIA) and about 20% (using PHOJET) for the sum of quasi-elastic and diffractive

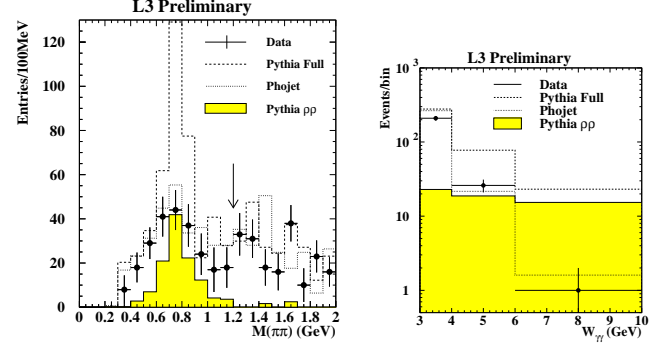


Figure 3: a) $\pi^+\pi^-$ mass distribution after background subtraction using wrong sign combination; b) number of 4π events as a function of $W = W_{\gamma\gamma}$.

events. In particular the acceptance for the quasi-elastic process $\gamma\gamma \rightarrow \rho\rho$ with all 4 pions in the central tracking detectors is extremely small at high W .

L3 has measured the rate of $\gamma\gamma \rightarrow \rho\rho$ events in the range $3 < W < 10$ GeV. The $\pi^+\pi^-$ mass distribution after background subtraction using wrong sign combinations and the number of 4π events as a function of W are shown in Fig. 1. The distribution is compared to the full PYTHIA and PHOJET simulation and to the PYTHIA simulation of $\gamma\gamma \rightarrow \rho\rho$ events. Both models do not contain any $\gamma\gamma \rightarrow \text{Resonance}$ processes which should also contribute in this mass region. From this study L3 concludes that both the rate and the W dependence of quasi-elastic processes are not properly simulated by PYTHIA.

2 Leading Order Parton Processes

The interaction of quasi-real photons ($Q^2 \approx 0$) studied at LEP and the interaction of a quasi-real photon with a proton studied at HERA (photoproduction) are very similar processes. In leading order (LO) different event classes can be defined in $\gamma\gamma$ and γp interactions. The photons can either interact as ‘bare’ photons (“direct”) or as hadronic fluctuation (“resolved”). Direct and resolved interactions can be separated by measuring the fraction x_γ of the photon’s momentum participating in the hard interaction for the two photons. In $\gamma\gamma$ interactions they are labelled x_γ^\pm for the two photons. Ideally, the direct $\gamma\gamma$ events with two bare photons are expected to have $x_\gamma^+ = 1$ and $x_\gamma^- = 1$, whereas for double-resolved events both values x_γ^+ and x_γ^- are expected to be much smaller than one. In photoproduction, the interaction of a bare photon with the proton is labelled ‘direct’ (corresponding to the ‘single resolved’ process in $\gamma\gamma$) and the interaction of a hadronic photon is called ‘resolved’ (corresponding to ‘double-resolved’ in $\gamma\gamma$).

3 Di-Jet Production in $\gamma\gamma$ Interactions

Studying jets should give access to the parton dynamics of $\gamma\gamma$ and γp interactions. OPAL has therefore measured di-jet production in $\gamma\gamma$ scattering at $\sqrt{s_{ee}} = 161 - 172$ GeV using the cone jet finding algorithm with $R = 1$ ⁹. Similar studies have been presented by the HERA experiments¹⁰. In di-jet events, x_γ^\pm is calculated using

$$x_\gamma^+ = \frac{\sum_{\text{jets}=1,2} (E + p_z)}{\sum_{\text{hadrons}} (E + p_z)} \quad \text{and} \quad x_\gamma^- = \frac{\sum_{\text{jets}=1,2} (E - p_z)}{\sum_{\text{hadrons}} (E - p_z)}, \quad (3)$$

where p_z is the momentum component along the z axis of the detector and E is the energy of the jets or hadrons.

For a given jet-jet centre-of-mass energy the cross-sections vary only with the scattering angle θ^* . The leading order direct process $\gamma\gamma \rightarrow q\bar{q}$ is mediated by t -channel spin- $\frac{1}{2}$ quark exchange which leads to an angular dependence $\propto (1 - |\cos\theta^*|)^{-1}$. In double-resolved pro-

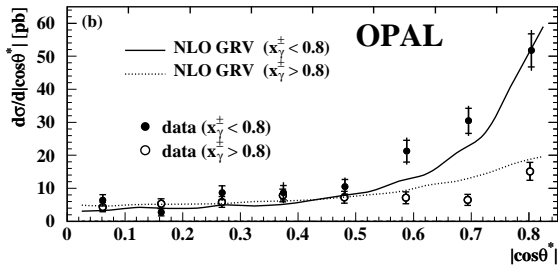


Figure 4: Angular distribution of di-jet events compared to NLO QCD calculations using the GRV parametrisation. The curves are normalised to the data in the first three bins. The invariant mass of the two-jet system must be larger than 12 GeV.

cesses all matrix elements involving quarks and gluons have to be taken into account, with a large contribution from spin-0 gluon exchange. After adding up all relevant processes, perturbative QCD predicts an angular dependence of approximately $\propto (1 - |\cos\theta^*|)^{-2}$. Fig. 4 shows the corrected $|\cos\theta^*|$ distribution of di-jet events with $x_\gamma^\pm > 0.8$ and with $x_\gamma^\pm < 0.8$ compared to a NLO calculation¹¹ which qualitatively reproduces the data.

The transverse momentum E_T^{jet} of the jet (or the final-state parton) defines a hard scale which can be used together with x_γ to constrain the parton densities $f(x_\gamma, E_T^2)$ of the photon. In the kinematic range covered by LEP the F_2^γ measurements are mainly probing the quark content of the photon¹², whereas di-jet production can be used to constrain the relatively unknown gluon distribution in the photon.

The E_T^{jet} distribution for di-jet events with pseudorapidities $|\eta^{\text{jet}}| < 2$ is shown in Fig. 5. The measure-

ments are compared to a NLO calculation¹³ which uses the NLO GRV parametrisation¹⁴. The direct, single- and double-resolved parts and their sum are shown separately. The data points are in good agreement with the calculation except in the first bin where theoretical and experimental uncertainties are large.

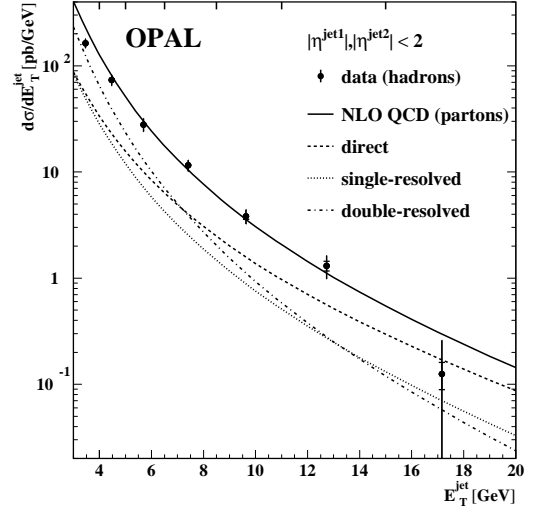


Figure 5: The inclusive e^+e^- di-jet cross-section as a function of E_T^{jet} for jets with $|\eta^{\text{jet}}| < 2$ using a cone size $R = 1$.

The x_γ distribution is shown in Fig. 6 in bins of \bar{E}_T^{jet} , where \bar{E}_T^{jet} is the mean value of the transverse energies of the two jets. No detector correction has been applied. The Monte Carlo predictions of PYTHIA and PHOJET are normalised to the number of data events. The contribution from direct processes, as predicted from PYTHIA, is also shown. The events from direct processes are concentrated at high x_γ values. As \bar{E}_T^{jet} increases, the x_γ distribution shifts to higher values and the fraction of direct events in the PYTHIA sample increases. The number of events is underestimated by PYTHIA and PHOJET by about 25 – 30%, if the predicted Monte Carlo cross-sections are taken into account, mainly for $x_\gamma < 0.9$.

The NLO QCD calculations do not take into account the possibility of an underlying event which leads to an increased jet cross-section. The underlying event is simulated in the Monte Carlo models PYTHIA and PHOJET which will be used to compare to different LO parametrisations of the parton distribution, GRV¹⁴, SaS-1D¹⁵ and LAC1¹⁶. In PYTHIA and PHOJET the modelling of the underlying event includes multiple interactions. A resolved photon contains several partons which can lead to multiple parton interactions in double-resolved events.

The contribution from multiple interactions has to be tuned using quantities which are not directly correlated to the jets, since otherwise effects of the parton distributions and of the underlying event cannot be dis-

OPAL

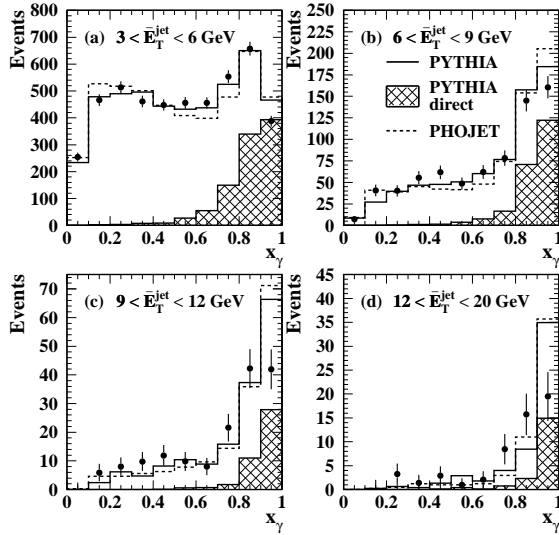


Figure 6: Uncorrected x_γ distribution in bins of the mean value of \bar{E}_T^{jet} for di-jet events with $E_T^{\text{jet}} > 3$ GeV and $|\eta^{\text{jet}}| < 2$. Each event is added to the plot twice, at the values of x_γ^+ and of x_γ^- . Statistical errors only are shown.

tinguished.

It is expected that the transverse energy flow outside the jets measured as a function of x_γ is correlated to the underlying event¹⁷. No effect due to the underlying event is expected for direct events at large x_γ . The increase of the transverse energy flow outside the two jets at small x_γ can therefore be used to tune the number of multiple interactions in the model.

The events were boosted into their centre-of-mass system and the transverse energy flow was measured as a function of x_γ in the central rapidity region $|\eta^*| < 1$. The regions around the jet axes with $R < 1.3$ are excluded from the energy sum. Fig. 7 shows the transverse energy flows corrected to the hadron level compared to the Monte Carlo models with different values of the parameter p_t^{mi} which defines the transverse momentum cutoff for multiple parton interactions. The following conclusion can be drawn:

- The influence of multiple interactions is small. The modelling of the transverse energy flow without multiple interactions is also consistent with the data.
- The optimised value of p_t^{mi} depends on the parametrisation used for the parton distributions. For all further comparisons with PYTHIA, the cut-off parameter p_t^{mi} was set to 2.5 GeV/c for LAC1, to 2.0 GeV/c for GRV and to 1.4 GeV/c for SaS-1D.

OPAL

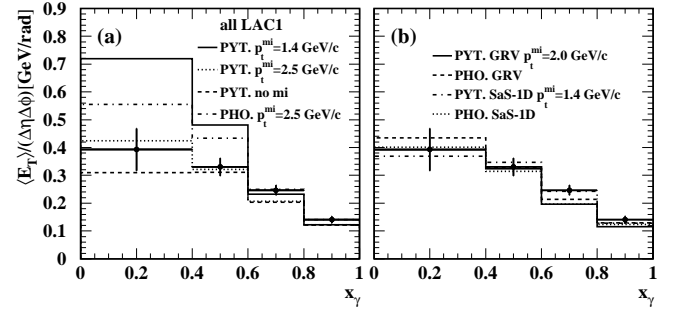


Figure 7: Transverse energy flow outside the jets in the central rapidity region $|\eta^*| < 1$ as a function of x_γ . The statistical error is smaller than the symbol size. The error bars show the statistical and systematic errors added in quadrature. The data are compared with the MC models using a) LAC1 and b) GRV and SaS-1D.

- PHOJET with either SaS-1D or GRV is in reasonable agreement with the data. Changing the default cutoff from $p_t^{\text{mi}} = 2.5$ GeV/c does not affect the transverse energy flow significantly.
- For γp collisions at HERA, $p_t^{\text{mi}} = 1.2$ GeV/c is the optimal choice with PYTHIA-GRV and $p_t^{\text{mi}} = 2.0$ GeV/c with PYTHIA-LAC1¹⁷. With these values the models slightly overestimate the transverse energy flows at low x_γ in the $\gamma\gamma$ data.

OPAL

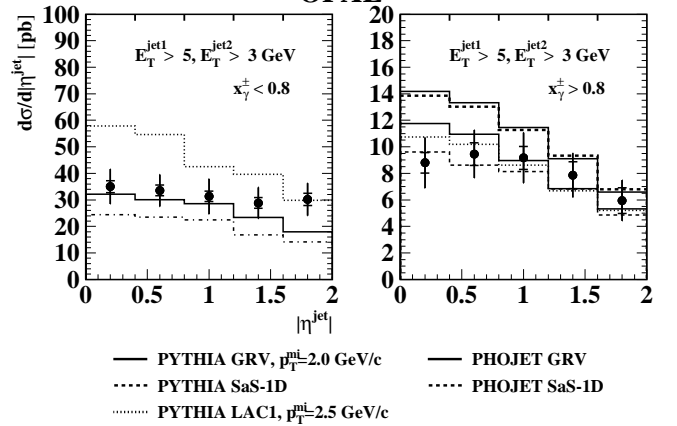


Figure 8: The inclusive two-jet cross-section as a function of $|\eta^{\text{jet}}|$ for events with $E_T^{\text{jet}1} > 4$ GeV and $E_T^{\text{jet}2} > 3$ GeV is shown for events with a) $x_\gamma^\pm < 0.8$ (mainly double resolved) and b) $x_\gamma^\pm > 0.8$ (mainly direct). Asymmetric E_T^{jet} cuts were chosen to avoid singularities in the NLO calculations (not shown).

After this optimisation of the description of the underlying event by the generators, the sensitivity of the jet cross-sections to the choice of parametrisation for the

parton distributions can be studied. The inclusive di-jet cross-section as a function of $|\eta^{\text{jet}}|$ for events with a large double-resolved contribution obtained by requiring $x_\gamma^\pm < 0.8$ is shown in Fig. 3a. The larger gluon density in LAC1 compared to SaS-1D and GRV in the $(x_\gamma, E_T^{\text{jet}})$ region probed here leads to an overestimation of the jet cross-section for double-resolved events. As expected, there exists almost no dependence on the choice of parametrisation for the mainly direct events with $x_\gamma^\pm > 0.8$ in Fig. 3b.

4 Hadron Production in $\gamma\gamma$ and γp Scattering

Measurements of hadron production cross-sections in $\gamma\gamma$ and γp scattering complement the studies of jet production. Hadron production at large transverse momenta is sensitive to the partonic structure of the interactions without the theoretical and experimental problem related to the various jet algorithms. Interesting comparisons of $\gamma\gamma$ and γp data taken at LEP and HERA, respectively, should be possible in the future, since similar hadronic centre-of-mass energies W of the order 100 GeV are accessible for both type of experiments.

4.1 Inclusive Charged Hadron Production in $\gamma\gamma$

The distributions of the transverse momentum p_T of hadrons produced in $\gamma\gamma$ interactions are expected to be harder than in γp or hadron-p interactions due to the direct component. This is demonstrated in Fig. 9 by comparing $d\sigma/dp_T$ for charged hadrons measured in $\gamma\gamma$ interactions by OPAL¹⁸ to the p_T distribution measured in γp and hp ($h = \pi, K$) interactions by WA69¹⁹. The

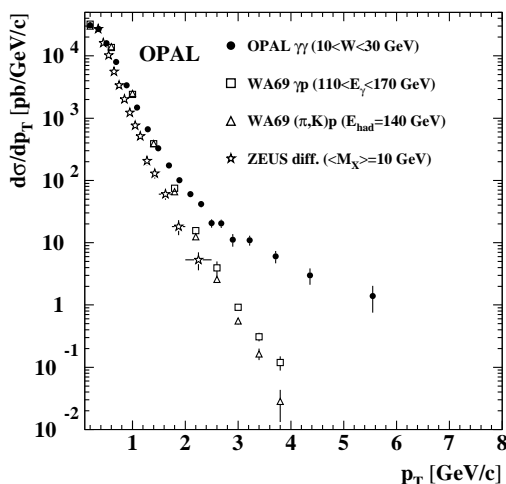


Figure 9: The p_T distribution measured in $\gamma\gamma$ interactions in the range $10 < W < 30$ GeV is compared to the p_T distribution measured in γp and hp ($h = \pi, K$) interactions by WA69¹⁹. The cross-section values on the ordinate are only valid for the OPAL data.

WA69 data are normalised to the $\gamma\gamma$ data in the low p_T region at $p_T \approx 200$ MeV/c using the same factor for the hp and the γp data. The hadronic invariant mass of the WA69 data is about $W = 16$ GeV which is of similar size as the average $\langle W \rangle$ of the $\gamma\gamma$ data in the range $10 < W < 30$ GeV.

Whereas only a small increase is observed in the γp data compared to the $h\pi$ data at large p_T , there is a significant increase of the relative rate in the range $p_T > 2$ GeV/c for $\gamma\gamma$ interactions due to the direct process.

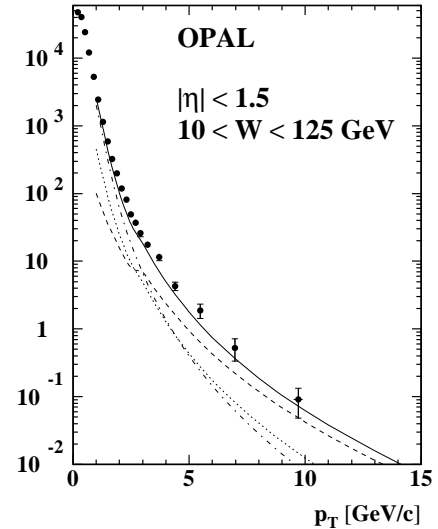


Figure 10: $d\sigma/dp_T$ for pseudorapidities $|\eta| < 1.5$ in the range $10 < W < 125$ GeV compared to NLO calculations for $p_T > 1$ GeV/c (continuous curve) together with the double-resolved (dot-dashed), single-resolved (dotted) and direct contributions (dashed).

The $\gamma\gamma$ data are also compared to a ZEUS measurement of charged particle production in γp events with a diffractively dissociated photon at $\langle W \rangle = 180$ GeV. The invariant mass relevant for this comparison should be the mass M_X of the dissociated system (the invariant mass of the ‘ γ -Pomeron’ system). The average $\langle M_X \rangle$ equals 10 GeV for the data shown. The p_T distribution falls exponentially, similar to the γp and hadron-p data, and shows no flattening at high p_T due to a possible hard component of the Pomeron.

The cross-sections $d\sigma/dp_T$ are also compared to NLO calculations²¹ which are calculated using the QCD partonic cross-sections, the NLO GRV parametrisation of the parton distribution functions¹⁴ and fragmentation functions fitted to e^+e^- data. The renormalisation and factorisation scales are set equal to p_T . The change in slope around $p_T = 3$ GeV/c in the NLO calculation is due to the charm threshold.

In Fig. 10, the NLO calculation is shown separately for direct, single- and double-resolved interactions. At large p_T the direct interactions dominate. The agreement

between the data and the NLO calculation is good.

4.2 Inclusive π^0 Production in γp

H1 has studied π^0 production in photoproduction by reconstructing the $\pi^0 \rightarrow \gamma\gamma$ decays using the new lead-scintillating fibre calorimeter SpaCal in the backward region (photon hemisphere)²². Fig. 11 shows the π^0 cross-

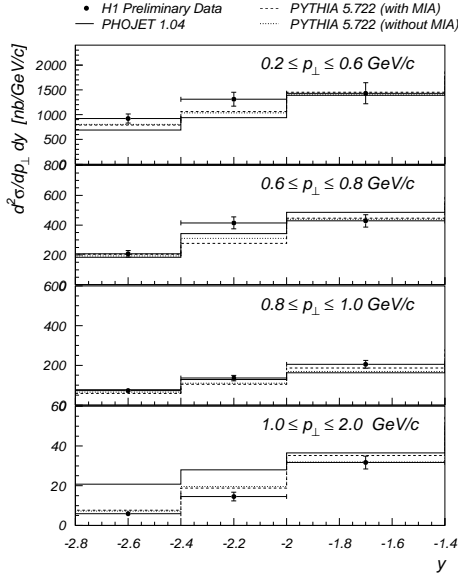


Figure 11: $d\sigma/dy$ for π^0 produced in γp interactions in different transverse momentum intervals. The results are compared to the PYTHIA and PHOJET predictions.

section as a function of the rapidity y together with the model predictions of PHOJET and PYTHIA. PYTHIA gives a better description of the data than PHOJET. The accuracy of the data is, however, not yet sufficient to distinguish multiple interaction models.

The differential cross-section $d\sigma/dp_T$ is presented in Fig. 12 together with H1 results on charged hadron production in the central pseudorapidity region ($|\eta| < 1.5$). Fitting an exponential and a power law function to the p_T spectrum shows that the low p_T region, $p_T < 1.3$ GeV, is well described by an exponential fall-off typical for soft hadronic interactions, but at high p_T a deviation is observed. In this region a power law function, which is typical for hard scattering processes, fits the data best.

5 Baryon-Antibaryon Asymmetry

It has been suggested by Kopeliovich and Povh²³ that the Baryon Number (BN) of the proton in γp scattering can either be carried by the valence quarks or by the sea quarks and gluons. The gluonic mechanism of BN

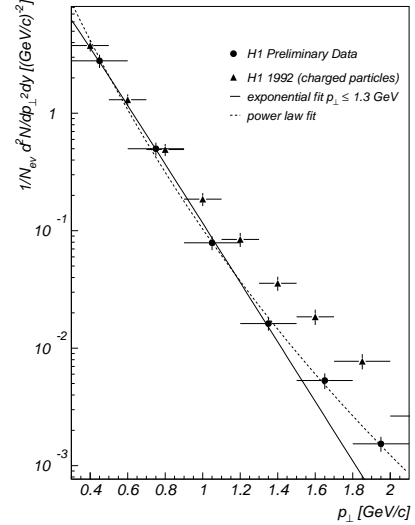


Figure 12: $d\sigma/dp_T$ for π^0 produced in γp interactions. The triangles indicate the H1 result on charged hadrons in the central rapidity region. The curves are different fits to the data.

transport proceeds through the production of baryon-antibaryon pairs in the photon fragmentation region.

H1 has studied this phenomenon in tagged photoproduction ($150 < W < 260$ GeV) by measuring the baryon-antibaryon asymmetry

$$A_B = 2 \frac{N_p - N_{\bar{p}}}{N_p + N_{\bar{p}}} \quad (4)$$

from the number of protons, N_p , and antiprotons, $N_{\bar{p}}$, per event²⁴. The theoretical expectation for the rapidity dependence of A_B is shown in Fig. 13.

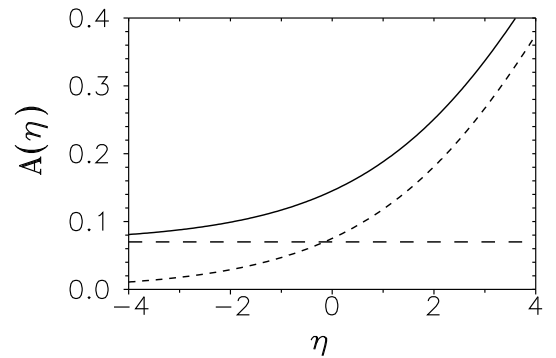


Figure 13: Baryon-antibaryon asymmetry $A_B(\eta)$ as a function of rapidity η for photoproduction at HERA²³. The dashed line corresponds to the gluonic mechanism of BN transfer and the dotted line to the quark mechanism which is peaked in the forward direction. The sum is shown as continuous line.

In the H1 detector, the (anti-)protons are identified by requiring that the measured energy loss, dE/dx , in

the Central Jet Chamber is twice the energy loss expected for a minimum ionising particle. Additional cuts reduce the background from beam-gas interactions and from secondary protons produced in the beam pipe. The baryon-antibaryon asymmetry is measured to be

$$A_B = 0.8 \pm 1.0(\text{stat}) \pm 2.5(\text{sys})\%$$

for (anti-)protons with momenta $0.3 < p < 0.6$ GeV/c and for polar angles $|\cos \theta| < 0.8$ ($|\eta| < 1.1$). The $\cos \theta$

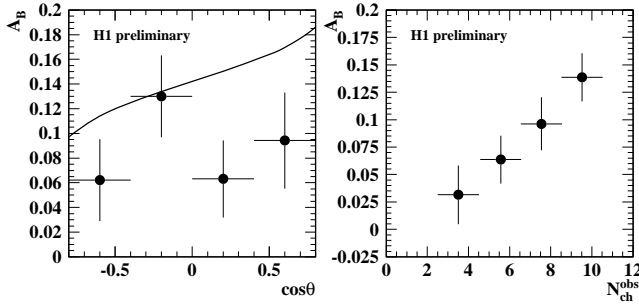


Figure 14: a) Baryon-antibaryon asymmetry A_B as a function of $\cos \theta$ compared to the model of Ref. 23; b) A_B as a function of the number of accompanying charged particles, $N_{\text{ch}}^{\text{obs}}$.

dependence of A_B is in qualitative agreement with the data in Fig. 14, yielding a non-vanishing asymmetry at about 7 rapidity units from the leading baryon production region. A quantitative comparison is not yet possible, since the (anti-)proton momentum cut and additional requirements on the multiplicity have not been applied in the model. In Fig. 14b, A_B is shown as a function of the number of accompanying charged particles, $N_{\text{ch}}^{\text{obs}}$, within the same angular interval as the (anti)-protons. The increase of A_B with $N_{\text{ch}}^{\text{obs}}$ is also in qualitative agreement with the expectation for the gluonic mechanism of BN transport.

6 Summary

The L3 and OPAL measurements of the total hadronic $\gamma\gamma$ cross-section are consistent. The measurements favour a stronger rise of the total cross-section with energy than observed in γp , pp or $\bar{p}p$ scattering.

The OPAL results on di-jet production in $\gamma\gamma$ scattering are well understood within the framework of perturbative NLO QCD. The di-jet cross-sections help to constrain the gluon content of the photon.

Comparisons of transverse momentum distributions measured in different processes yield information about the partonic structure of the interactions.

A first H1 measurement of a non-vanishing baryon asymmetry in the photon hemisphere is in qualitative agreement with the gluonic mechanism of baryon number transport.

Acknowledgements

I want to thank Maria Kienzle (L3), Martin Erdmann, Andrey Rostovtsev and Martin Swart (all H1) for their help in preparing this presentation.

References

1. S.E. Baru et al., *Z. Phys. C* **53**, 219 (1992); TPC/ 2γ Coll., H. Aihara et al., *Phys. Rev. D* **41**, 2667 (1990); TPC/ 2γ Coll., D. Bintinger et al., *Phys. Rev. Lett.* **54**, 763 (1985); PLUTO Coll., Ch. Berger et al., *Phys. Lett. B* **149**, 421 (1984).
2. L3 Coll., paper 519 submitted to this conference; M. Acciarri et al., *Phys. Lett. B* **408**, 450 (1997).
3. OPAL Coll., paper 199 submitted to this conference.
4. Review of Particle Physics, *E. Phys. J. C* **3**, 1 (1998).
5. A. Donnachie, P.V. Landshoff, hep-ph/9806344.
6. A. Corsetti et al., Proc. of PHOTON '97, Egmond aan Zee, NL (1997); M. Drees, R.M. Godbole, *Nucl. Phys. B* **339**, 355 (1990); *Z. Phys. C* **59**, 591 (1993); J.R. Forshaw, J.K. Storrow, *Phys. Rev. D* **46**, 4955 (1992).
7. G. A. Schuler, T. Sjöstrand, *Z. Phys. C* **677**, 73 (1997).
8. R. Engel, J. Ranft, *Phys. Rev. D* **54**, 4244 (1996).
9. OPAL Coll., paper 198 submitted to this conference (hep-ex/9808027).
10. G. Grindhammer, L. Sinclair, these proceedings.
11. M. Klasen et al., hep-ph/9712256, and private communication.
12. K. Freudenreich, these proceedings.
13. T. Kleinwort, G. Kramer, *Nucl. Phys. B* **477**, 3 (1996); PLB **370**, 141 (1996); M. Klasen, private communication.
14. M. Glück et al., *Phys. Rev. D* **45**, 3986 (1992); *Phys. Rev. D* **46**, 1973 (1992);
15. G.A. Schuler, T. Sjöstrand, *Z. Phys. C* **68**, 607 (1995).
16. H. Abramowicz et al., *Phys. Lett. B* **269**, 458 (1991).
17. H1 Coll., S. Aid et al., *Z. Phys. C* **70**, 17 (1996).
18. OPAL Coll., paper 197 submitted to this conference (hep-ex/9808009).
19. R.J. Apsimon et al., *Z. Phys. C* **43**, 63 (1989).
20. ZEUS Coll., M. Derrick et al., *Z. Phys. C* **67**, 227 (1995).
21. J. Binnewies et al., *Phys. Rev. D* **53**, 6110 (1996).
22. H1 Coll., paper 576 submitted to this conference.
23. B. Kopeliovich, B. Povh, *Z. Phys. C* **75**, 693 (1997).
24. H1 Coll., paper 556 submitted to this conference.